

This work was written as part of one of the author's official duties as an Employee of the United States Government and is therefore a work of the United States Government. In accordance with 17 U.S.C. 105, no copyright protection is available for such works under U.S. Law.

Public Domain Mark 1.0

<https://creativecommons.org/publicdomain/mark/1.0/>

Access to this work was provided by the University of Maryland, Baltimore County (UMBC) ScholarWorks@UMBC digital repository on the Maryland Shared Open Access (MD-SOAR) platform.

Please provide feedback

Please support the ScholarWorks@UMBC repository by emailing scholarworks-group@umbc.edu and telling us what having access to this work means to you and why it's important to you. Thank you.

AERONET—A Federated Instrument Network and Data Archive for Aerosol Characterization

B. N. Holben,^{*} T. F. Eck,[†] I. Slutsker,[‡] D. Tanré,[§] J. P. Buis,^{||} A. Setzer,[¶]
 E. Vermote,^{**} J. A. Reagan,^{††} Y. J. Kaufman,^{*} T. Nakajima,^{‡‡} F. Lavenu,^{§§}
 I. Jankowiak,[§] and A. Smirnov[‡]

The concept and description of a remote sensing aerosol monitoring network initiated by NASA, developed to support NASA, CNES, and NASDA's Earth satellite systems under the name AERONET and expanded by national and international collaboration, is described. Recent development of weather-resistant automatic sun and sky scanning spectral radiometers enable frequent measurements of atmospheric aerosol optical properties and precipitable water at remote sites. Transmission of automatic measurements via the geostationary satellites GOES and METEOSATS' Data Collection Systems allows reception and processing in near real-time from approximately 75% of the Earth's surface and with the expected addition of GMS, the coverage will increase to 90% in 1998. NASA developed a UNIX-based near real-time processing, display and analysis system providing internet access to the emerging global database. Information on the system is available on the project homepage, <http://spamer.gsfc.nasa.gov>. The philosophy of an open access database, centralized processing and a user-friendly graphical interface has contributed to the growth of international cooperation for ground-based aerosol monitoring and imposes a stan-

dardization for these measurements. The system's automatic data acquisition, transmission, and processing facilitates aerosol characterization on local, regional, and global scales with applications to transport and radiation budget studies, radiative transfer-modeling and validation of satellite aerosol retrievals. This article discusses the operation and philosophy of the monitoring system, the precision and accuracy of the measuring radiometers, a brief description of the processing system, and access to the database. ©Elsevier Science Inc., 1998

INTRODUCTION

Accurate knowledge of the spatial and temporal extent of aerosol concentrations and properties has been a limitation for assessing their influence on satellite remotely sensed data (Holben et al., 1992) and climate forcing (Hansen and Lacis, 1990). With the exception of the AVHRR weekly ocean aerosol retrieval product (Rao et al., 1989), the voluminous 20-year record of satellite data has produced only regional snapshots of aerosol loading, and none have yielded a database of the optical properties of those aerosols that are fundamental to our understanding of their influence on climate change. With the advent of the EOS era of laboratory quality orbiting spectral radiometers, new algorithms for global scale aerosol retrievals and their application for correction of remotely sensed data will be implemented (Kaufman and Tanré, 1996). However, the prospect of fully understanding aerosols influence on climate forcing is small without validation and augmentation by ancillary ground-based observations as can be provided by radiometers historically known as sun photometers. Following is a description of a new Sun-sky scanning radiometer system that standardizes ground-based aerosol measurements and pro-

^{*} NASA/Goddard Space Flight Center, Greenbelt

[†] Hughes STX Corporation, Code 923, NASA/GSFC, Greenbelt

[‡] Science Systems and Applications Inc., Code 923, NASA/GSFC, Greenbelt

[§] Laboratoire d'Optique Atmosphérique, U.S.T. de Lille, Villeneuve d'Ascq, France

^{||} CIMEL Electronique, Paris, France

[¶] Instituto de Pesquisas Espaciais, Sao José dos Campos, Brazil

^{**} University of Maryland, NASA/GSFC, College Park

^{††} University of Arizona, Tucson

^{‡‡} University of Tokyo, Komaba, Meguro-ku, Tokyo, Japan

^{§§} Laboratoire d'Ecologie, Ecole Normale Supérieure, Paris, France

Address correspondence to Brent Holben, NASA/GSFC, Code 923, Greenbelt, MD 20771. E-mail: brent@kratmos.gsfc.nasa.gov

Received 30 May 1997; revised 12 February 1998.

cessing, can provide much of the ground-based validation data required for future remote sensing programs and may provide basic information necessary for improved assessment of aerosols impact on climate forcing.

BACKGROUND

The technology of ground-based atmospheric aerosol measurements using sun photometry has changed substantially since Volz (1959) introduced the first handheld analog instrument almost 4 decades ago. Modern digital units of laboratory quality and field hardiness can collect data more accurately and quickly and are often interfaced with onboard processing (Schmid et al., 1997; Ehsani et al., 1998; Forgan, 1994; Morys et al., 1998). The method used remains the same, that is a filtered detector measures the spectral extinction of direct beam radiation according to the Beer–Lambert–Bouguer law:

$$V_{\lambda} = V_0 d^2 \exp(\tau_{\lambda} m) t_y \quad (1)$$

where

- V =digital voltage,
- V_0 =extraterrestrial voltage,
- m =optical air mass,
- τ =total optical depth,
- λ =wavelength,
- d =ratio of the average to the actual Earth–Sun distance,
- t_y =transmission of absorbing gases.

The digital voltage (V) measured at wavelength (λ) is a function of the extraterrestrial voltage (V_0) as modified by the relative Earth–Sun distance (d), and the exponent of the total spectral optical depth (τ_{λ}) and optical air mass (m). The total spectral optical depth is the sum of the Rayleigh and aerosol optical depth after correction for gaseous absorption.

The multifilter rotating shadowband radiometer (MFRSR) employs a different strategy. It measures spectral total and diffuse radiation to obtain the direct component from which aerosol optical thickness is computed using the Beer–Lambert–Bouguer law. The instrument nominally measures at 1-min intervals and has been shown to be reliable over long periods of time. The measurements are networked to a common server by a modem interface and the data processed by a common analysis system (Harrison et al., 1994). It is widely used in the United States principally for the DOE ARM sites. As the number of measurements from the MFRSR network increases, the impact of aerosol loading on the radiation balance should be more clearly understood, especially when taken in concert with other ground, airborne, and satellite measurements.

Sky scanning spectral radiometers, that is, radiometers that measure the spectral sky radiance at known angular distances from the Sun, have expanded the aerosol

knowledge base most importantly through inversion of the sky radiances to derive aerosol microphysical properties such as size distribution and optical properties such as phase function (Nakajima et al., 1983; 1996; Tanré et al., 1988; Shiobara et al., 1991; Kaufman et al., 1994). This technique requires precise aureole measurements near the solar disk and good straylight rejection. Historically these systems are rather cumbersome, not weather-hardy, and expensive. The CIMEL and PREDE (French and Japanese manufacturers, respectively) Sun and sky scanning spectral radiometers overcome most such limitations, and provide retrievals from direct Sun measurements of aerosol and water vapor abundance in addition to aerosol properties from inversion of spectral sky radiances. Since the measurements are directional and represent conditions of the total column atmosphere, there are direct applications to satellite and airborne observations as well as atmospheric processes.

As has been demonstrated by the shadowband network and satellite remote sensing in general, prompt delivery of the data for analysis is fundamental for obtaining a comprehensive, continuous database, and allows assessment of the collecting instruments health and calibration. To achieve this goal, minimize costs and expand the coverage globally, we use the simple and inexpensive Data Collection System (DCS) operating on the geosynchronous GOES, METEOSAT, and GMS satellites providing nearly global coverage in near real-time at very little expense (NOAA/NESDIS, 1990).

Finally there are the very contentious issues of processing the data archive. Although the Beer–Lambert–Bouguer law is very straightforward, its implementation has as many variations as there are investigators who use it. The central problem being agreement on the accuracy by which the aerosol optical thickness is derived. The uncertainties in computation of the air mass (m), the calculations for the Rayleigh and ozone optical depths (τ_r , τ_o), and water vapor expressed as total column abundance or precipitable water (Pw) as well as strategies for calibration of the instruments and monitoring the long-term change in calibration all combine to preclude any globally accepted processing scheme. Perhaps even more debatable are the aerosol properties derived from inversions of the sky radiances with the radiation transfer equation. Our solutions make the raw data and calibration data available to the user and provide a basic processing package (of published, widely accepted algorithms) with sufficient friendliness and flexibility that all data may be accessed globally through common forms of electronic communication on the internet.

Following is the Aerosol Robotic Network (AERONET) version of a ground-based aerosol monitoring system that offers a standardization for a ground-based regional to global scale aerosol monitoring and characterization network. We have assembled a reliable system and offer it as a point of focus for further development

of each component. As an example of the system's performance under a variety of conditions, we present data collected in the Brazilian Amazon during the dry season and Mauna Loa, Hawaii. Owing to the fundamental importance of these and similar data for basic aerosol research, aerosol forcing research and validation of retrievals from space-based platforms, we are emphasizing this system for a regional to global scale network of these observations. Our philosophy is for an open, honor system whereby all contributed data may be accessed by anyone, but publication of results requires permission of the contributing investigators. We have designed and implemented a system that promotes these goals.

AUTOMATIC SUN AND SKY SCANNING SPECTRAL RADIOMETER

Most if not all sun photometer networks have had limited success when people are required to make routine observations. Therefore, an automatic instrument is a fundamental component for routine network observations. The measurement protocol must be reasonably robust such that unwanted data may be successfully screened from useful data, data quality, and instrument functionality may be evaluated and the instrument should be self-calibrating or at the least collects data for its calibration. Following is our assessment of the CIMEL CE-318 instrument that meets these criteria of a field hardy, transmitting, Sun, and sky scanning spectral radiometer which is used in the AERONET program.

General Description

The CIMEL Electronique 318A spectral radiometer manufactured in Paris, France is a solar-powered weather hardy robotically pointed sun and sky spectral radiometer. This instrument has approximately a 1.2° full angle field of view and two detectors for measurement of direct sun, aureole, and sky radiance. The 33 cm collimators were designed for 10^{-5} straylight rejection for measurements of the aureole 3° from the sun. The robot-mounted sensor head is parked pointed nadir when idle to prevent contamination of the optical windows from rain and foreign particles. The Sun/aureole collimator is protected by a quartz window allowing observation with a UV enhanced silicon detector with sufficient signal-to-noise for spectral observations between 300 nm and 1020 nm. The sky collimator has the same field of view, but an order of magnitude larger aperture-lens system allows better dynamic range for the sky radiances. The components of the sensor head are sealed from moisture and desiccated to prevent damage to the electrical components and interference filters. Eight ion-assisted deposition interference filters are located in a filter wheel which is rotated by a direct drive stepping motor. A thermister measures the temperature of the detector

allowing compensation for any temperature dependence in the silicon detector. A polarization model of the CE-318 is also used in AERONET. This version executes the same measurement protocol as the standard model but takes additional polarized solar principal plane sky radiance measurements hourly at 870 nm (Tables 1 and 2).

The sensor head is pointed by stepping azimuth and zenith motors with a precision of 0.05° . A microprocessor computes the position of the Sun based on time, latitude, and longitude, which directs the sensor head to within approximately 1° of the Sun, after which a four-quadrant detector tracks the Sun precisely prior to a programmed measurement sequence. After the routine measurement is completed, the instrument returns to the "park" position awaiting the next measurement sequence. A "wet sensor" exposed to precipitation will cancel any measurement sequence in progress. Data are downloaded under program control to a Data Collection Platform (DCP) typically used in the geostationary satellite telemetry system (see Data Transmission section).

Measurement Concept

Since the instrument was first available in 1992, the measurement protocols have evolved to a point in which we feel maximum information content is achieved within the constraints of the hardware and software available for the network system and the goals of the aerosol climatology data base. The radiometer makes only two basic measurements, either direct Sun or sky, both within several programmed sequences. The direct Sun measurements are made in eight spectral bands (anywhere between 340 nm and 1020 nm; 440 nm, 670 nm, 870 nm, 940 nm, and 1020 nm are standard) requiring approximately 10 s. A sequence of three such measurements are taken 30 s apart, creating a triplet observation per wavelength. Triplet observations are made during morning and afternoon Langley calibration sequences and at standard 15-min intervals in between (Table 1). The time variation of clouds are typically greater than that of aerosols, causing an observable variation in the triplets that can be used to screen clouds in many cases. Additionally the 15-min interval allows a longer temporal frequency check for cloud contamination.

Sky measurements are performed at 440 nm, 670 nm, 870 nm, and 1020 nm (Table 1). A single spectral measurement sequence (Langley sky) is made immediately after the Langley air mass direct Sun measurement, 20° from the Sun. This is used to assess the stability of the Langley plot analysis according to O'Neill and Miller (1984). Two basic sky observation sequences are made, the "almucantar" and "principal plane." The philosophy is to acquire aureole and sky radiances observations through a large range of scattering angles from the Sun through a constant aerosol profile to retrieve size distribution, phase function, and aerosol optical thickness

Table 1. Measurement Sequences of the CIMEL Sun/Sky Scanning Spectral Radiometer

	Spectral Range (nm)	Target	No. Obs.	Obs. Interval	Application
Basic direct Sun	340–1020	Sun	1 each λ	~ 8 s for 8 λ	AOT, Pw, a
Triplet observation	340–1020	Sun	Three direct sun	3 at 30 s apart, 1 min total	AOT, Pw, a and cloud screening
Standard measurement sequence	340–1020	Sun	Variable: depends on day length	Ea. 15 min, $m=2$ a.m. to $m=2$ p.m.	AOT, Pw, a
Langley	340–1020	Sun	16, a.m. and p.m. between $m=7$ and 2	$m=7-5$, incr. of 5 m; $m=5-2$, incr. of 25 m	Langley, Cal, AOT, Pw, a
Basic sky	440–1020	Sky	1 each λ	None	Sky radiance
Langley sky	440–1020	Sky	16 between $m=7$ and 2	$m=7-5$, 0.5; $m=5-2$, 0.25	Stability of Langley plot
Almucantar	440–1020	Sky	72 (Table 2)	>8 /day: $m=4, 3, 2, 1.7$ hrly 9 a.m. to 3 p.m.	Size dist. and $P(\theta)$, AOT, a
Polarization	870	Sky	42 (Table 2)	Hourly; 9 a.m. to 3 p.m.	Size dist. and $P(\theta)$
Principal plane	440–1020	Sky	42 (Table 2)	Hourly; 9 a.m. to 3 p.m.	Size dist. and $P(\theta)$, AOT, a

(AOT). An almucantar is a series of measurements taken at the elevation angle of the Sun for specified azimuth angles relative to the position of the Sun. The range of scattering angles decrease as the solar zenith angle decreases; thus almucantar sequences made at an optical airmass of 2 or more achieve scattering angles of 120° or larger. Scattering angles of 120° are typical of many sunsynchronous viewing satellites; thus a measure of the satellite path radiance is approximated from the ground station. During an almucantar measurement, observations from a single channel are made in a sweep at a constant elevation angle across the solar disk and continues through 360° of azimuth in about 40 s (Table 2). This is repeated for each channel to complete an almucantar sequence. More than four almucantar sequences are made daily at an optical airmass of 4, 3, 2, and 1.7 both morning and afternoon and, an almucantar is made hourly between 9 a.m. and 3 p.m. local solar time for the standard instrument and skipping only the noon almucantar for the polarization instrument. A direct Sun observation is made during each spectral almucantar sequence.

The standard principle plane sequence measures in much the same manner as the almucantar but in the principal plane of the Sun where all angular distances from the Sun are scattering angles regardless of solar zenith angle. This measurement sequence begins with a sun observation, moves 6° below the solar disk, and then sweeps through the sun taking about 30 s for each of the four spectral bands (Table 2). Principal plane observations are made hourly when the optical airmass is less than 2 to minimize the variations in radiance due to the change in optical airmass.

Polarization measurements of the sky at 870 nm are an option with this instrument. The sequence is made in the principal plane at 5° increments between zenith angles of -85° and $+85^\circ$. The configuration of the filter wheel requires that a near-IR polarization sheet is attached to the filter wheel. Three spectrally matched 870 nm filters are positioned in the filter wheel exactly 120° apart. Each angular observation is a measurement of the three polarization filter positions. An observation takes approximately 5 s and the entire sequence about 3 min. This sequence occurs immediately after the standard principle plane measurement sequence.

Instrument Precision

We define the precision of the instrument as its ability to accurately reproduce results from multiple measurements under constant conditions using standardized techniques. Three methods will be used to assess the radiometric precision: 1) the variability of the digital numbers (DN) from the spectral response acquired from the 2-m-diameter integrating sphere at Goddard Space Flight Center, which is used to determine the gain and offset calibrations of the sky radiance channels, 2) examination

Table 2. Almicantar and Principal Plane Sequences for the Standard and Polarization Instruments

	Sun	Sky (deg)
Almicantar—azimuth angle relative to Sun	0°	6.0, 5.0, 4.5, 4.0, 3.5, 3.0, 2.5, 2.0, -2.0, -2.5, -3.0, -3.5, -4.0, -4.5, -5.0, -6.0, -8.0, -10.0, -12.0, -14.0, -16.0, -18.0, -20.0, -25.0, -30.0, -35.0, -40.0, -45.0, -50.0, -60.0, -70.0, -80.0, -90.0, -100.0, -110.0, -120.0, -130.0, -140.0, -160.0, -180.0
Principal plane: standard— scattering angle from Sun (negative is below the Sun)	0°	Duplicate above sequence for a complete counter clockwise rotation to -6 -6.0, -5.0, -4.5, -4.0, -3.5, -3.0, -2.5, -2.0, 2.0, 2.5, 3.0, 3.5, 4.0, 4.5, 5.0, 6.0, 8.0, 10.0, 12.0, 14.0, 16.0, 18.0, 20.0, 25.0, 30.0, 35.0, 40.0, 45.0, 50.0, 60.0, 70.0, 80.0, 90.0, 100.0, 110.0, 120.0, 130.0, 140.0
Principal plane: polarization— zenith angle (negative is in the antisolar direction)	—	-85.0, -80.0, -75, -70, -65.0, -60.0, -55.0, -50.0, -45.0, -40.0, -35.0, -30.0, -25.0, -20.0, -15.0, -10.0, -5.0, 5.0, 10.0, 15.0, 20.0, 25.0, 30.0, 35.0, 40.0, 45.0, 50.0, 55.0, 60.0, 65.0, 70.0, 75.0, 80.0, 85.0

of dark current values taken during each sky radiance measurement, and 3) the triplet variability of the DNs taken from Mauna Loa Observatory Langley observations was used to evaluate the sun channels.

All instruments are routinely calibrated with Goddard's 2-m integrating sphere at least twice per year and the reference instruments approximately monthly. Each calibration session consists of three sequential measurements at four lamp levels (radiance levels). The sphere's precision is not well known however the absolute accuracy is $\sim 5\%$ or less (Walker et al., 1991). Assuming the sphere has perfect precision, we may use these data to estimate the precision of the sky channels. The percent deviation from the mean of each sequence was averaged from all the sequences since 1993 for each of the three reference instruments. In all but one case, the variability was much less than 1% of the mean value (Table 3A). Given these results, some of the variability in Table 3A could be attributed to the uncertainty in the precision of the integrating sphere and the potential for variability in the data collection procedure.

Over 3000 dark current values were examined for each instrument and the average values computed by wavelength for the Sun and both sky (aureole $2-6^\circ = \text{sky}^1$ and dark sky $6-180^\circ = \text{sky}^2$) observations. The dark current values for the Sun observations averaged less than 1 count compared to typical measurement values of 2000 to 15,000 counts, depending on wavelength, optical depth, and air mass (Table 3B); thus for typical conditions the dark current is insignificant. The sky observations have a higher dark current value ranging from 2 to 14 counts with standard deviations of approximately the same magnitude. Typically this is about 1% of the signal and is subtracted prior to radiance computation.

Langley plots from NOAA's Mauna Loa Observatory have been made to determine the spectral extraterrestrial voltage ($V_{0\lambda}$) for these instruments since 1993. The observatory's high altitude and isolation from most local and regional sources of aerosols provides a very stable aerosol and irradiance regime in the mornings (Shaw, 1983). The Langley plot is a log of the DN taken during these times plotted against the optical air mass between

a range of 5 and 2. The intercept is the calibration coefficient, and the slope the optical thickness. If the aerosol loading is constant, these points plot as a straight line. The deviation of these points from the linear regression line is a measure of the precision of the instrument, although it does include atmospheric variation, which we are assuming is negligible at Mauna Loa during the selected Langleys. Table 3C shows the average variability of a triplet is less than 1% and is most typically 0.3% for all three instruments. This is in agreement with the precision estimated from the integrating sphere analysis.

Instrument Calibration

Calibration refers to the determination of the calibration coefficients needed to convert the instrument output (DN) to a desired output, in this case aerosol optical thickness (AOT) and radiance ($\text{W/m}^2/\text{sr}/\mu\text{m}$). The calibration accuracy is the level of accuracy with which a desired output is achieved using defined comparison procedures. Calibration is frequently traced back to the variability with which the calibration coefficients are determined to achieve that unit output. Thus instrument calibration is a combination of the instrument precision, the calibration procedure, and the algorithms used. In this section, we will discuss the variability of the calibration coefficients we determine for the sky channels from the 2-m integrating sphere, the spectral V_0 from the Mauna Loa Langleys, and the change in the calibration coefficients as a function of time. We will also discuss the intercomparison procedure for transferring the V_0 calibration coefficients from a reference instrument to a field instrument and the computation of the resultant variability.

The sphere calibration procedure given in the previous section allows us to compute a gain and offset for each sky wavelength. The mean dark current DN is typically between 0 and 14 counts (the median DN is 0 to 1 for the Sun channels) (Table 3B) which is subtracted from the DN thus giving an offset of 0. The Instrument DNs are plotted against the exitant radiance from the integrating sphere, and a gain is computed from the linear regression fit through the origin. The mean gain is com-

Table 3. The DNs Used To Compute A) the % Variation from the Mean for the Sky Channels, B) the Mean Dark Current Values for All Measurement Conditions, and C) the % Variation of the Mean Triplet Values during Selected Mauna Loa Langley Plots for Three Field and Reference Instruments^a

A) Integrating Sphere															
λ (μm)	Inst. #2					Inst. #13					Inst. #32				
	Mean % var.				n	Mean % var.				n	Mean % var.				n
	1.02	0.87	0.67	0.44		1.02	0.87	0.67	0.44		1.02	0.87	0.67	0.44	
12 Lamps	—	—	0.1	0.3	3	—	—	0.1	0.1	9	—	—	0.5	0.3	4,8
6 Lamps	2.7	0.8	0.7	0.4	7	—	0.5	0.1	0.1	9	0.1	0.1	0.1	0.2	8
2 Lamps	0.2	0.3	0.2	0.3	8	0.1	0.1	0.1	0.2	9	0.3	0.2	0.2	0.3	8
1 Lamp	0.1	0.1	0.1	0.4	7	0.1	0.1	0.1	0.4	9	0.1	0.1	0.1	0.4	8

B) Dark Current															
	Inst. #2				n	Inst. #13				n	Inst. #32				n
	Mean DN			n		Mean DN			n		Mean DN			n	
	Sun	Sky ¹	Sky ²			Sun	Sky ¹	Sky ²			Sun	Sky ¹	Sky ²		
1020 nm	1.17	11.98	7.16	3201		1.29	6.01	4.00	3889		0.43	14.04	8.00	2703	
940 nm	0.64	—	—	3201		0.22	—	—	3889		0.05	—	—	2703	
870 nm	0.73	8.07	4.36	3201		0.59	3.62	2.87	3889		0.21	9.17	6.17	2703	
670 nm	0.56	4.52	2.02	3201		0.15	1.93	1.14	3889		0.11	6.40	4.15	2703	
440 nm	0.60	4.94	2.10	3201		0.15	2.02	1.16	3889		0.10	5.57	3.31	2703	
380 nm	0.56	—	—	3201		0.01	—	—	3889		0.06	—	—	2703	
340 nm	0.77	—	—	3201		0.23	—	—	3889		0.05	—	—	2703	

C) Mauna Loa Langley Plots							
Sun	Inst. #2		n	Inst. #13		n	
	Mean var. (%)			Mean var. (%)			
1020 nm	0.2		288	0.3		168	264
940 nm	0.2		288	0.3		168	264
870 nm	0.3		288	0.4		168	264
670 nm	0.3		288	0.3		168	264
440 nm	0.3		288	0.3		168	264
380 nm	0.7		288	0.5		168	264
340 nm	0.9		288	0.7		168	264

^aSky¹=small aperture collimator for measurements from 2° to 6° from Sun; Sky²=large aperture collimator for measurements from 6° to 180° from Sun.

puted from three regression gains made for each session. The accuracy of the sphere is reported as $\pm 5\%$ (Walker et al., 1991); thus the calibration coefficient accuracy can be no better than 5% plus the variability of the three regressions (precision) or conservatively $\pm \sim 5.5\%$. (Unpublished studies of the 2-m integrating sphere in 1997 indicate the absolute accuracy is between 1% and 3% depending on wavelength.)

The V_0 calibration coefficients are typically computed from an average of five or more Langley plots obtained at the Mauna Loa Observatory. The variability of the retrieved mean V_0 as measured by the coefficient of variation (CV, standard deviation/mean) indicates the combined uncertainty of the atmosphere, instrument, and the repeatability of the calibration procedure. The averaged Mauna Loa Langleys V_0 obtained during all calibration sessions have a CV of ~ 0.25 – 0.50% for the visible and near-IR wavelengths, ~ 0.5 – 2% for the UV to ~ 1 – 3% for the water vapor channel (Table 4 and continuing observations).

The Mauna Loa (MLO) calibration is conducted with two simultaneously operating reference instruments. Comparisons are made between ratios of raw spectral voltages as a check for instrument repeatability. A diurnal variation of less than 1% of the ratioed voltages is considered acceptable. Approximately monthly, the MLO master instruments are swapped with two reference instruments located at GSFC. The GSFC reference instruments are used for intercomparison with field instruments. Monitoring voltage ratios is continued for all master instruments and field instruments during the calibration procedure.

With respect to the long term stability of the calibration coefficients, the optical interference filters are the limiting factors. Periodic sphere gains and mountain top Langley calibration coefficients have been determined since 1993. The results are typical for interference filters. On average, there has been a decrease from 1% to 5% per year and, after 2 years, there has been a rapid decay in some filters (Table 5). However, starting in 1997 we

Table 4. The Mean CV in Percent by Wavelength (nm) of the Mauna Loa Derived Langley V_0 for All of the Wavelengths Used in the Reference CIMEL Sun Photometers

Inst. No.	1020 (CV%)	940 (CV%)	870 (CV%)	670 (CV%)	500 (CV%)	440 (CV%)	380 (CV%)	340 (CV%)
2	0.19	2.39	0.14	0.18	0.22	0.22	0.35	2.10
13	0.27	0.89	0.29	0.44	0.90	0.40	0.77	0.63
32	0.26	3.19	0.19	0.24	0.23	0.29	1.10	0.48
37	0.29	2.23	0.21	0.32	0.28	0.28	0.32	0.43
101	0.26	0.70	0.40	0.23	0.10	0.22	0.32	0.37

installed ion-assisted deposition (IAD) interference filters in all instruments with the expectation of improved filter stability with time, which in fact is noted in Table 5 for instrument #11. Since the percentage decrease in the time dependent calibration coefficients is usually greater than the uncertainty of a semiannual V_0 determination, we use a linear interpolation of the V_0 between calibration dates. This requires that the instrument calibration coefficient be followed closely. Thus, until more information is available, we calibrate instruments on a 6-month rotation and change filters after 2 years of field use. Therefore, the percentage changes which occur between V_0 calibrations are actually a factor of 2–3 smaller than shown in Table 5 since these values are on a percentage change per year.

Most instruments cannot be calibrated at Mauna Loa, and a well calibrated integrating sphere with sufficient radiometric output is not common; therefore, most instruments are calibrated at Goddard Space Flight Center with the 2-m integrating sphere and intercomparisons against the Goddard reference instrument with a Mauna Loa-derived V_0 . Intercomparisons are made by solving Eq. (1) for the field instrument V_0 based on the reference instrument τ_a during simultaneous observations (time difference of less than 5 s), under clear stable atmospheric conditions (τ_{a440} less than 0.15). The CV of the V_0 computed from these comparisons is typically larger than the reference instrument uncertainty. The total error is the uncertainty attributed to the field instrument calibration coefficient due to transfer of calibration from the reference instrument plus the error from the refer-

ence instrument defined from the Mauna Loa calibration. As with the reference instruments, calibration coefficients are then linearly interpolated between the calibration tie points unless independent information suggests a different method as in the case of a change in filters at which time new calibration comparisons must be made. The spectral voltage ratios of the field instrument are compared to the reference instruments during several days. Variations throughout a large range of optical air mass (typically 1.5–6) of less than $\pm 1\%$ are considered acceptable.

Measurements of the spectral temperature sensitivity of the instrument in a temperature-controlled chamber showed agreement with the manufacturers published temperature sensitivity of the detectors. To date, only the 1020 nm channels showed significant temperature variation ($0.25\%/^{\circ}\text{C} \pm 0.05\%/^{\circ}\text{C}$) warranting a correction to a reference temperature in the processing. However, for polarization instruments, measurements indicate that the plastic polarizing filter introduces a temperature sensitivity of $\sim 0.20\%/^{\circ}\text{C}$ to the polarized 870 nm radiance measurements.

Data Accuracy

Various instrumental, calibrational, atmospheric, and methodological factors that influence the precision and accuracy of optical depth determination have been pointed out clearly in a series of publications (Shaw, 1976; Reagan et al., 1986; Russel et al., 1993), and attempts to account for or minimize these are described in previous sections. Instrument uncertainty due to elec-

Table 5. The Decay Rate of Zero Air Mass Voltages, V_0 (%/yr), Shown for Filters Less than 2 Years Old for Each Reference Instrument

	1020	940	870	670	500	440	380	340
#2								
6–10/95	–2	–1	2	2	3	–4	11	3
#13								
6–9/94	5	–31	2	0	ND	2	23	11
#13								
9/94–6/95	10	5	10	11	ND	15	20	15
#32								
6–10/95	4	6	7	2	2	4	26	5
#11								
6/97–1/98	–4	8	–1	0	0	0	–3	–2

Table 6. The Absolute Value (and % Error) of the Extinction Optical Depth and Scattering Optical Depth at Air Mass of 2 Clearly Illustrate the Possible Advantages of Using the Scattering Optical Depth for Low Optical Depth Ranges

Calibration Error	0%	1%	5%
τ_{ext}	0.059 (0%)	0.058 (1%)	0.056 (5%)
τ_{ext}	0.059 (0%)	0.054 (8.5%)	0.033 (44.1%)

troptical precision is for all practical purposes insignificant (Table 3) for a properly operating instrument. The variability of the atmosphere is characterized by the variability of the triplet optical thicknesses which may at times be cloud contaminated. This uncertainty is computed, can be used as a screening tool, and may be retrieved from the AERONET data base. Additionally the uncertainty due to calibration is tracked with all time-dependent data and may also be retrieved from the database. Typically the total uncertainty in AOT from a newly calibrated field instrument under cloud-free conditions is $<\pm 0.01$ for $\lambda > 440$ nm and $<\pm 0.02$ for shorter wavelengths. Uncertainty in the water vapor retrieval is limited by larger uncertainty in the V_0 for the 940 nm channel and by the uncertainty of the radiosonde inter-comparisons, typically less than 12%.

The uncertainty of the sky radiance data is more difficult to ascertain since these only constitute single observations and no absolute self-calibration procedure is implemented between the sphere calibrations. Based on the sphere calibration, the uncertainty in the sky radiance at the time of calibration is assumed $<\pm 5\%$ for all four channels at the time of calibration. Scattering aerosol optical depth is directly related to the aureole brightness and thus the accuracy is a function of the sky calibration. We feel that for low optical depth monitoring the sky brightness may retrieve scattering optical depths with less absolute error than traditional extinction approaches (Table 6), assuming perfect straylight rejection and a uniformly distributed aerosol in the aureole. Development of an *in situ* sky calibration procedure is under evaluation (Nakajima et al., 1996).

DATA TRANSMISSION

Data are transmitted from the memory of the sun photometer via the Data Collection Systems (DCS) to the geostationary satellites GOES-E, GOES-W, or METEOSAT (GMS is anticipated in 1998) and then retransmitted to the appropriate ground receiving station. The data can be retrieved for processing either by modem or Internet linkage, resulting in near real-time acquisition from almost any site on the globe excluding poleward of 80° latitude. The DCS is a governmental system operated for the purpose of transmitting low volume environmental

data from remote sites for various institutions and government agencies.

Each station on the GOES and METEOSAT networks has been assigned a user ID and transmission time window passing up to 30 kbytes per day in 24 and 48 individual transmissions at hourly and half-hourly intervals, respectively. During each transmission, a packet of data and status information are time stamped by the radiometer, the transmitter and the central receiving station (Wallops Island, VA, USA for GOES; Darmstadt, Germany for METEOSAT; and Tokyo, Japan for GMS). Typically the data are maintained in the receiving station computers for 3–5 days before they are overwritten. The data are retrieved daily from the central receiving station which we term near real-time.

PROCESSING SYSTEM

A fundamental component of the AERONET system is a package of user-friendly UNIX software that provides near real-time information on the status and calibration of the instruments, data processing with referenced and generally accepted processing algorithms, an orderly archive of the data, and convenient electronic access for all users to the raw and processed database. We shall discuss these aspects of the current operational state of the software and future enhancements.

Instrument and Network Status

The radiometer data stream includes date, time, temperature, battery voltage, wet sensor status, and time of transmission as well as several levels of identification numbers. The DCP adds a time stamp at the time of transmission as does the DCS receiving station plus checks for parity errors and signal strength of the transmission. After data are downloaded from the central receiving station, a status report and a trouble shooting report are automatically generated and e-mailed to appropriate system and instrument managers, and an internet homepage provides these information to the entire community. The status report provides a comprehensive assessment of the operation of the radiometer and DCP for the data transmitted with the current download. Network managers then have sufficient information to assess the operation of individual stations. To more quickly identify trouble spots, a troubleshooting report is generated that lists by instrument only information that fails to meet normal operating thresholds, that is, low battery voltage, transmission time error, missed transmission, etc. This approach can identify remote station problems quickly, often leading to same day resolution. Documentation of the status report is available under the AERONET homepage <http://spamer.gsfc.nasa.gov>.

Table 7. The Algorithms, Inputs, Corrections, and Models Used in Computing the Aerosol Optical Thickness, Pw, Spectral Irradiance, and Sky Radiance Inversions are Referenced

Variable, Algorithm or Correction	Comments	References
<i>Basic Computations</i>		
Rayleigh optical depth τ_r refractive index of air depolarization factor	Input elevation in m	Penndorf, 1957 Edlen, 1966 Young, 1980 Burcholtz, 1995 Michalsky, 1988 Iqbal, 1983
Solar zenith angle θ_0 Earth–Sun distance d Ozone amount O_3	Table lookup by 5° lat. long.	London et al., 1976 Kasten and Young, 1989 Kasten and Young, 1989 Komhyr et al., 1989
Aerosol optical air mass m_a Rayleigh optical air mass m_r O_3 optical air mass m_o		
<i>Corrections</i>		
Temperature T Water vapor for 1020 AOT Rayleigh, all wavelengths O_3 abs. coef. $\lambda > 350$ nm O_3 abs. coef. $\lambda < 350$ nm Time t	~0.25%/°C for 1020 nm specific for each inst. From Pw retrieval, Lowtran From elevation Cimel, UTC, DAPS time stamps, ± 1 s	Hamamatsu Inc. and Lab measurements Kneizys et al., 1988 Vigroux, 1953 Bass and Paur, 1984 Refer to Homepage
<i>Retrievals</i>		
Spectral direct Sun AOT, Langley plots Pw: (a , k , V_0) Scattering AOT Size dist., phase function Size dist.	Beer's Law Modified Langley From spectral sky radiance From spectral sky radiance From spectral direct sun AOT	Shaw, 1983 Bruegge et al., 1992; Reagan et al., 1992 Nakajima et al., 1983 Nakajima et al., 1983 Twitty, 1975; Halthore and Fraser, 1987, King, 1978
<i>Models</i>		
Spectral2 (irradiance) 6-S (linkage)	Parametrized spectral RT Analytical, RT	Bird and Riordan, 1986 Vermote et al., 1996
<i>Procedures</i>		
Cloud screening Climatology, direct sun Climatology, sky	Thresholds, λ AOT and t AOT, Pw, wavelength exp. Size dist., phase function g	Refer to Homepage Refer to Homepage Refer to Homepage

Data Processing

There is lack of agreement on corrections, calibration procedures, data analysis procedures, etc. often caused by divergent error tolerances or specific requirements of various investigators. We have implemented a series of processing algorithms on a UNIX server that have been published in the open literature and/or are generally accepted by the scientific community (Table 7). These algorithms impose a processing standardization on all of the data taken in the network facilitating comparison of spatial and temporal data between instruments. The archival system allows the user community to access either the raw or processed data via internet for examination, analysis, and/or reprocessing as needed. The archival browse algorithms are collectively known under the program name “demonstrat,” which graphically provides access to all aspects of the database and through the AERONET homepage (<http://spamer.gsfc.nasa.gov>). The program operates on a workstation called “spamer.gsfc.nasa.gov”. The algorithms within “demonstrat” comprise three principal categories; time dependent retrievals such as AOT and Pw, calibration assessment, and sky ra-

diance retrievals. There are a growing number of sub processing algorithms within each of these. As importantly, “demonstrat” allows all data to be retrieved through “FTP” and e-mail access for personal computer analysis and/or reprocessing as the user requires. As new and improved approaches and models are accepted within the community, the processing may be applied uniformly to the network-wide database. Additionally access to the database through “demonstrat” provides an opportunity for testing new algorithms and models for an increasingly diverse set of measurements for a variety of locations and conditions. The following figures were obtained directly from the “demonstrat” output to illustrate the access to the database.

Archival Browser (“Demonstrat”)

The custom browser “demonstrat” allows a comprehensive method of viewing and screening the data in either raw or processed form. Following are a few of the options available in demonstrat that we feel are important for use in a network data base.

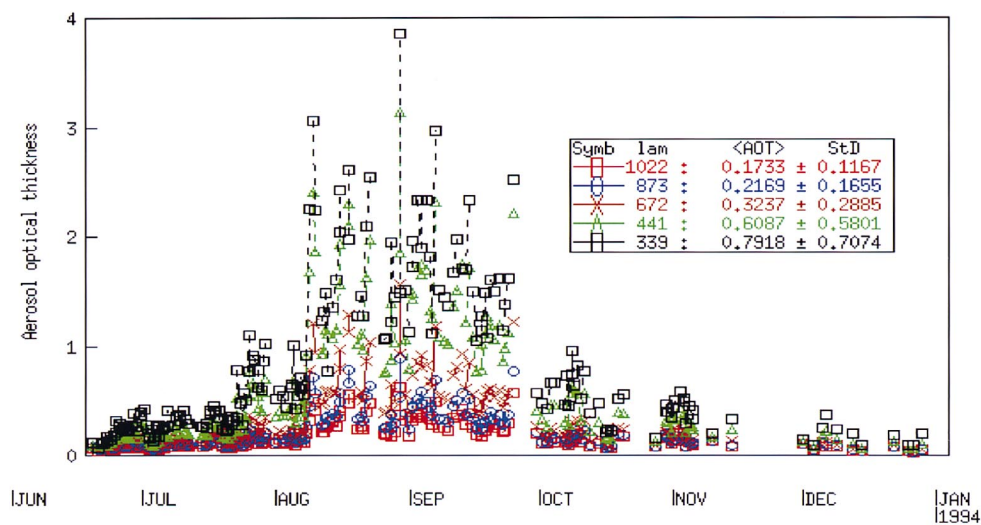


Figure 1. The aerosol optical thickness dry season record for Cuiaba, Brazil showing a large increase in August and September 1993 due to region wide burning.

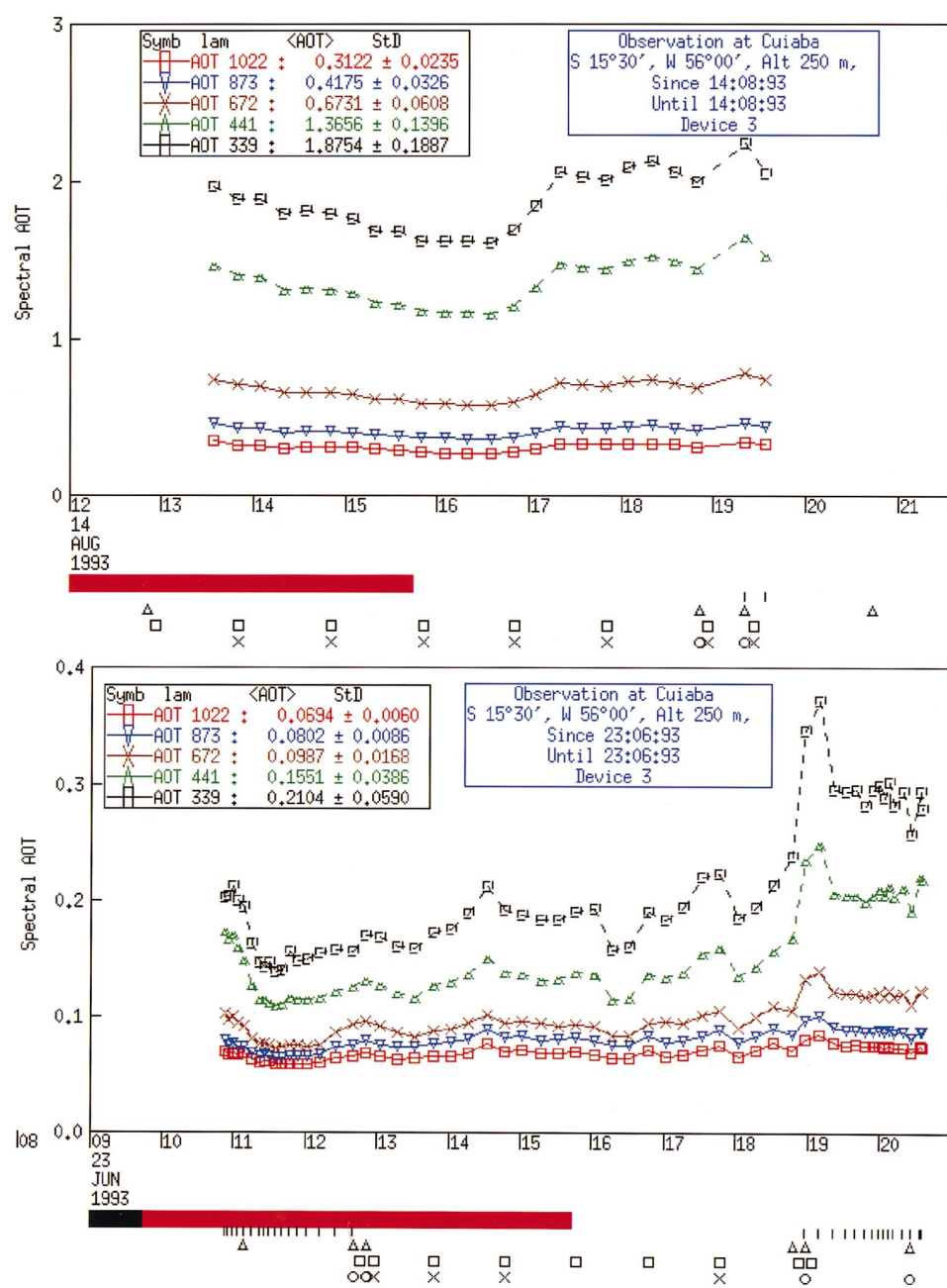


Figure 2. The aerosol optical thickness in Cuiaba on 14 August 1993 (top) shows significant aerosol loading in contrast to 23 June (bottom). Note the addition of time-dependent information on the abscissa including almucantar (Δ), principal plane (\square), inversion (\circ or \times), and Langley data ($|$).

Time Dependent AOT Retrievals

The time dependence window serves as the access point for all other windows. The aerosol optical thickness, precipitable water, wavelength exponent, and calibration coefficient trends as well as the status indicators (battery voltage, temperature, and wet sensor) may be plotted as a function of time in this window. For a particular instrument and location, all or part of the data may be displayed by interactive cursor subsetting. For example, the dry season data (June to October) from Cuiaba, Brazil (Holben et al., 1996) clearly shows the increase in aerosol optical thickness as the burning season begins in August (Fig. 1). Subsetting to 8 days of data or less, the UTC time scale and a local time bar are drawn, the mean 15-min direct Sun AOT observations are plotted and almucantar (triangles), principle plane (squares), and successful inversions (o and x) are shown under the time scale (Fig. 2). A hatched line above the time scale indicates Langley data, and vertical bars inside the plot indicate that the wet sensor has been activated and no sun data are available. Individual points may be rejected in these windows.

Calibration Assessment

Historically, uncertainty due to calibration of sun photometers has limited their wide scale deployment and long-term use. No new methods are offered; however, “demonstrat” imposes a standard computation of aerosol optical thickness and Pw calibration coefficients and in so doing renders a simple method via a graphics window for the user to assess the quality of these calibration coefficients interactively from the online database. Two windows were implemented for standardizing the direct Sun calibration coefficient procedure and assessing their quality control. The first is the traditional Langley plot with the modified Langley method used for water vapor retrieval. A second method is a simple intercomparison.

The radiometer acquires a Langley data sequence each morning and afternoon between an optical airmass of 2 and 7. The interactive calibration routine allows manual rejection of data points and automatically computes a table of V_0 's for each wavelength. Tabled V_0 's are recomputed and displayed after each rejection. The V_0 's may be applied to the original Langley data and aerosol optical thickness plotted as a function of time or air mass in two additional windows for further inspection of the quality of the Langley plot. The water vapor calibration coefficient determined by the modified Langley method (Bruegge et al., 1992; Reagan et al., 1992) is performed in much the same way. The water vapor transmittance is modeled from each 940 nm filter function using MODTRAN and has been shown to be largely independent of temperature and water vapor profiles (Halthore et al., 1997). Both Langley methods are typically used only for absolute calibration analysis with more restrictive airmass ranges from high mountain top acquisitions for our refer-

ence instruments. This is particularly important for the UV and 940 nm (water vapor) wavelengths.

An intercomparison algorithm searches a specified portion of the database for space and time coincidence (Fig. 3) of two instruments. Sun data are automatically intercompared by spectral aerosol optical thickness. A table of old and new calibration coefficients is generated from which an assessment for further calibration is made.

The history of the calibration coefficient determinations for each instrument is easily tracked on demand by a calibration tree showing the date, location, and reference instrument from which each intercomparison was made, back to a mountain top Langley or sphere calibration. Additionally a time dependent plot of the calibration coefficients shows the trends over time for the instrument in question.

Sky Radiance Inversions

The almucantar window displays the four channel sky radiances as a function of scattering angle, volume size distribution from 0.1 μm to $\sim 8.0 \mu\text{m}$, scattering phase function, and a table of the aerosol optical thickness and wavelength exponent computed from both direct Sun and the aureole measurements (Figs. 4a, 4b). Additionally the spectral asymmetry factor is computed from the phase function. From the radiance data, a window may be opened with zoom capabilities which separates the four spectral sky radiance bands into single color coded bands allowing close inspection of the data. The program automatically checks the quality of the almucantar data by examining the symmetry of the aureole radiances about the Sun. If the angular asymmetry defined as $|(l-r)/(l+r)*0.5|$, where l =left side and r =right side radiance pairs, exceeds 10%, those pairs are removed from the inversion process. If the standard deviation of the difference between aureole pairs divided by the averaged value of the angular pairs exceeds 10% or there are not a sufficient number of data points remaining with symmetry (10), the data are not inverted. The inversion routine used is that of Nakajima et al. (1983) and has a number of options that will be implemented over time. This will include size distribution inversions by combining the spectral optical thickness from direct Sun measurements and aureole data. In cases where the almucantar or principle plane data are not available, an interactive inversion from the spectral AOT data can be made, but the retrieved size range will be smaller due to reduced sensitivity to large particles.

The principle plane data are processed using the same inversion; however, only data on the zenith side from the solar disc are used in the inversion due to asymmetry induced by the ground reflectance and an increasingly large optical airmass. The principle plane window has identical capabilities as the almucantar window. The test for the quality of the data is simply the smoothness of the curve.

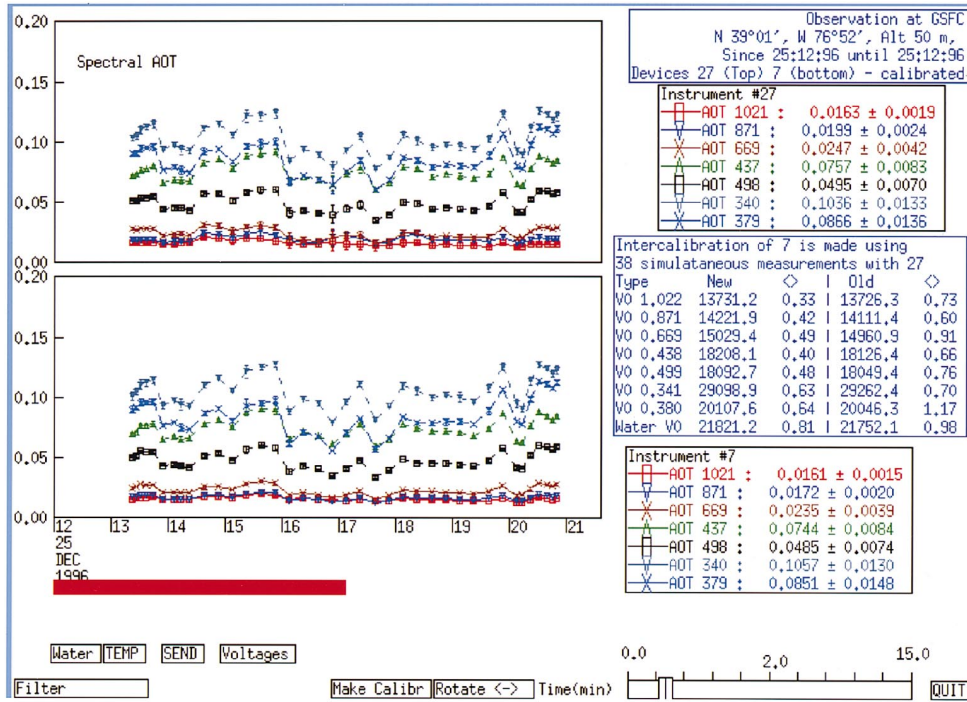


Figure 3. The intercomparison window which allows recomputation of V_0 values from a time series of AOTs of two simultaneously measuring instruments. AOTs from a reference instrument (top plot) are used with voltages from a field instrument (bottom plot) to compute a table of new V_0 's. Options to examine time-dependent voltage ratios may also be accessed from this window.

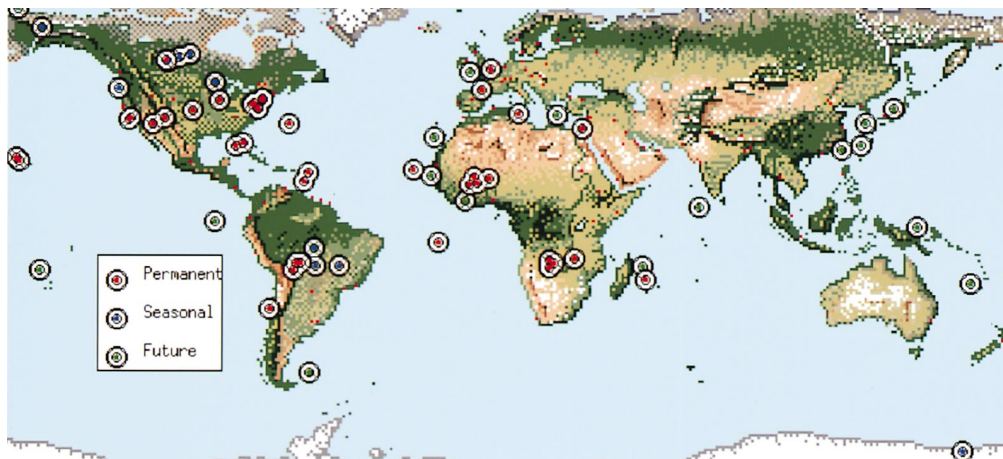
Radiative Transfer Model Interface

We have incorporated a parametrized spectral cloud-free flux model SPECTRAL2 (Bird and Riordan, 1986) to compute the total, direct, and diffuse down welling flux in the total solar spectrum and photosynthetically active radiation (PAR) bands from the measured aerosol and water vapor measurements. Single scattering albedo is the only required parameter which the instrument does not measure and thus must be supplied by the user. The interactive computations are made for any instantaneous or time dependent measurements. The window displays the spectral flux curves for the total, direct, and diffuse

irradiance, and a summary box gives integrated values for each component of the broad band (0.3–4.0 μm) and PAR (0.4–0.7 μm). The model is applied to the time dependence creating a data set of integrated fluxes. Options exist to compute coincident fluxes for user specified background conditions. Ratios of ambient vs. background conditions are computed and displayed in a summary box.

An interface to the more rigorous 6S model has been developed. The size distribution parameters $[dV(r)/d \log r \approx r^4 dN(r)/dr]$ deduced from the almucantar inversion as well as the index of refraction (imaginary and real) can easily be input to the 6S model (Vermote et

Figure 5. The approximate location of instruments is represented by the colored circles. Measurements are made at permanent sites year round. Data are taken seasonally at high latitudes and/or when cloud cover permits. In 1997 nearly 60 locations contributed to the database.



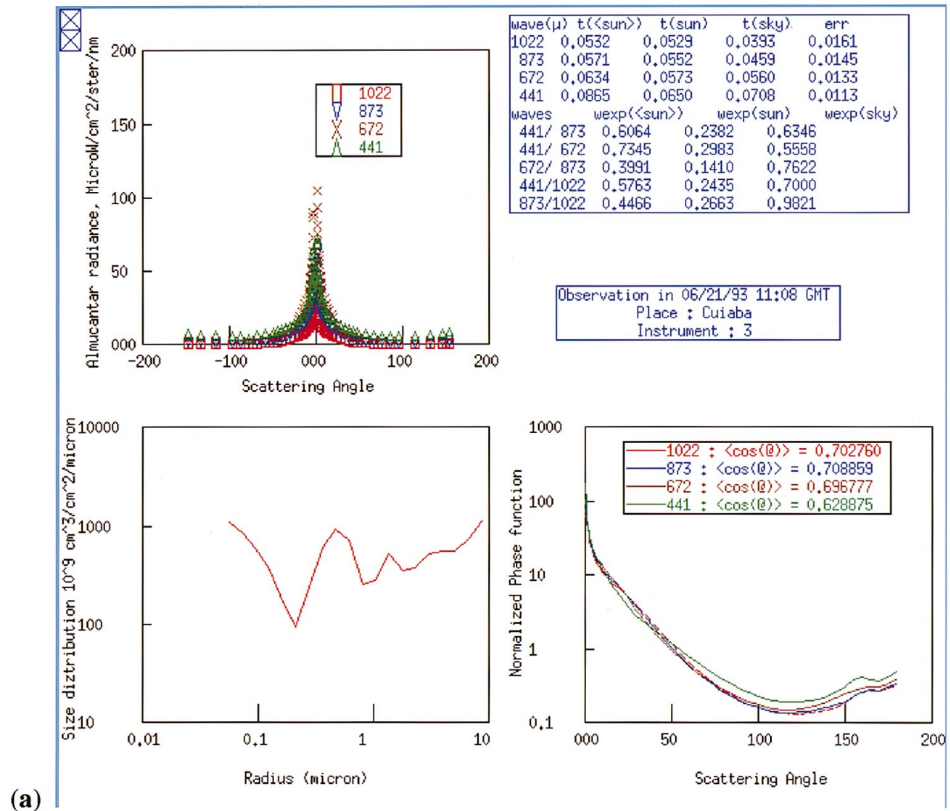


Figure 4a. A successful inversion of almucantar radiances during low aerosol loading and high aerosol loading.

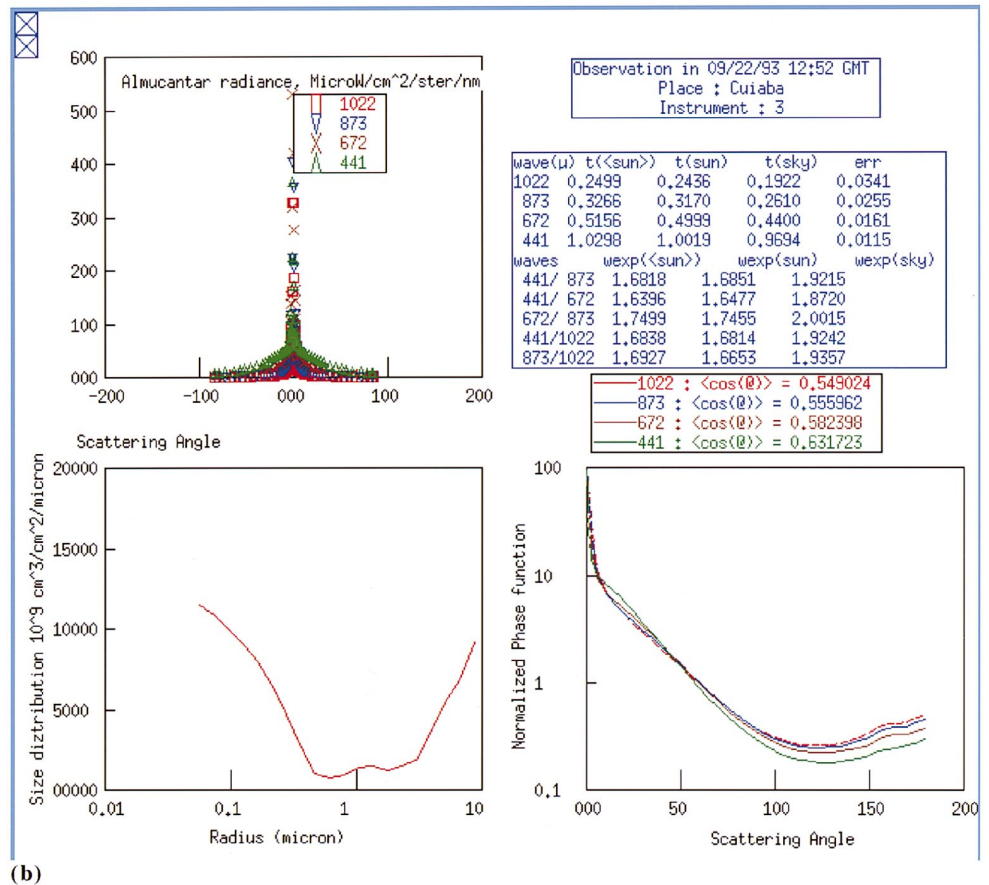


Figure 4b. A successful inversion of almucantar radiances during low aerosol loading and high aerosol loading is possible when the radiance data are symmetric about the Sun (upper left plot within window). Inversions produce a volume size distribution with good accuracy from 0.1 μm to about 8 μm aerosol radii (lower left window). The aerosol optical thickness and wavelength exponent are computed (upper right window) and compared to that measured by direct Sun observation. The spectral phase function and asymmetry factor (lower right side of window) from the aureole inversion are also computed using the “pakrad” code of Nakajima et al. (1996).

al., 1997) and used to compute the phase function, extinction, and scattering coefficient at any wavelength between $0.25\ \mu\text{m}$ and $4.0\ \mu\text{m}$. These quantities are then used to generate a large set of atmospheric parameters in addition to the simulation of the signal observed from aircraft or space by a variety of sensors. The computation of the phase function and extinction is done by the MIE subroutine [described in details in Vermote et al. (1996)]. Computations are restricted to the case of the scattering of electromagnetic waves by a mixture of homogeneous isotropic spheres, the physical properties of particles whose sizes are comparable to or larger than the wavelength. These assumptions are in accordance with those used in the sun photometer size distribution retrieval algorithm.

Cloud Screening

Data are taken by the automatic instruments under all nonprecipitation conditions causing significant cloud contamination in some of the raw data. Two approaches are used. The cloud contaminated database available through *demonstrat* provides for the user simple cloud screening tools based on the variability of the triplets and for continental nondust aerosols the spectral dependence of the AOT. Despite these screenings, some cloud contaminated data will be displayed, and further screening is left to the user. A second data base has been generated based on a series of triplet variability, time-dependent tests, and thresholds to automatically screen the database and provide a basic quality control of the database (Smirnov, 1998).

Automatic cloud screening of the almucantar and principal plane data are by symmetry and smoothness checks respectively of the data about the solar disc as explained under “sky radiance inversions.”

Downloading Data

Labeled spreadsheet export files may be created during a “*demonstrat*” browser session of all raw or processed data in the database and all data processed during a session, for example, modeled fluxes. Data for export may be selected by location, time, and the type of raw or processed data desired. The data may be downloaded to any computer with Internet access through the AERONET homepage, using a guest account or may be e-mailed directly during a “*demonstrat* session.” Homepage data access is under development and is expected to be the primary mode for data access in the near future.

The public domain database has developed as an honor system among the numerous contributing PIs according to the following requirement: Analysis and publication of any part of the data base by non-PIs requires permission of the owner. We recognize that this tenet is the key to expanding the AERONET database and expect the scientific community to honor it. The owner is identified when the data are retrieved through the homepage or *demonstrat*.

GLOBAL PERSPECTIVE

Through 1997 approximately 100 instruments have been included in the network and 60 instruments were deployed world-wide on various islands, North America, South America, Europe, Africa, and the Middle East, fostered by collaboration between international, national, and local agencies, private foundations, and individuals (Fig. 5). As the database continues to expand, the processing system becomes more sophisticated, and more users have access to the database, the need to provide better access to and quality assurance of the database becomes more critical. To aid in that effort, the reference data base is located on “*spamer.gsfc.nasa.gov*” at Goddard Space Flight Center in Greenbelt, Maryland, USA or “*loaser.univ-lille1.fr*” (IP number is 134.206.50.10) at Laboratoire d’Optique Atmosphérique, U.S.T. de Lille, 59655-Villeneuve d’Ascq, France for European access. A third supported data base will be established in Tokyo, Japan to support access to the data from eastern Asia. Identical clones of these systems have been established at various locations to facilitate access to the data for local activities. All processing changes are made to the entire *spamer* reference database to maintain uniform processing.

An automatic, computerized quality assured database is available and is continuing to be improved providing a screened data set to the scientific community. It is accessed by a simplified version of the “*demonstrat*” browser, “*demonstrat II*,” available through the AERONET homepage. The data must exceed specified optical, radiometric, and calibrational specifications as well as incorporating screening algorithms for cloud contamination that are functionally related to temporal and spectral behavior of the aerosol optical depth. Further details will be included in the homepage.

The network is expected to provide characterization of aerosol optical properties, a database for atmospheric correction, validation of satellite-based aerosol retrievals, and satellite observations of ocean color. The simple technology and international collaboration that has produced AERONET can be expanded to complimentary data sets of BRDF, automatic lidar systems, and radiation networks.

CONCLUSION

We believe that a successful system for long-term monitoring and characterization of aerosols requires automatic low maintenance radiometers, real time data reception, and processing as well as an easily accessible database for the scientific community. We have combined commercially available hardware, international agency collaborations, a public domain software, and a collaborative philosophy among investigators to form a network that has yielded regionally based aerosol amounts and proper-

ties in North and South America, Africa, the Middle East, and various Atlantic and Pacific islands. More systems will come online in the years ahead that will provide greater spatial coverage and synergism between and satellite measurements to achieve the objectives of specific intensive field campaigns and global climate change assessment. The philosophy of an open interactive database is expected to promote research and collaboration among investigators.

The authors wish to thank Diane Wickland and Tony Janetos of NASA Headquarters for providing the initial support for this project, Michael King of NASA's EOS Project Science Office for continued support, Chris Justice for contributing to the vision of the network, and John Vande Castle and Gunar Fedosejevs for actively participating in development of the network. Many thanks to Bruce Forgan for his detailed constructive recommendations to this manuscript and the other anonymous reviewers for their useful comments. Numerous others have contributed significant time, resources and funds to this effort; our thanks to them.

REFERENCES

- Bass, A. M., and Paur, R. J. (1984), The ultraviolet cross-section of ozone: 1. The measurements. In *Atmospheric Ozone* (C. S. Zerefos and A. Ghazi, Eds.), Reidel, Dordrecht, pp. 606–610.
- Bird, R. E., and Riordan, C. (1986), Simple solar spectral model for direct and diffuse irradiance on horizontal and tilted planes at the Earth's surface for cloudless atmospheres. *J. Clim. Appl. Meteorol.* 25:87–97.
- Bruegge, C. T., Conel, J. E., Green, R. O., Margolis, J. S., Holm, R. G., and Toon, G. (1992), Water vapor column abundance retrievals during FIFE. *J. Geophys. Res.* 97(D19):18,759–18,768.
- Burcholtz, A. (1995), Rayleigh-scattering calculations for the terrestrial atmosphere. *Appl. Opt.* 34:2765–2773.
- Edlen, B. (1966), The refractive index of air. *Meteorology* 2:71–80.
- Ehsani, A. R., Reagan, J. A., and Erxleben, W. H. (1998), Design and performance analysis of an automated 10-channel solar radiometer instrument. *J. Atmos. Ocean. Tech.* 15: 697–707.
- Forgan, B. W. (1994), General method for calibrating Sun photometers. *Appl. Opt.* 33:4841–4850.
- Halothore, R. N., and Fraser, R. S. (1987), Inversion of aerosol optical thickness measurements to obtain aerosol size distribution using Twitty's method, unpublished manuscript.
- Halothore, R. N., Eck, T. F., Markham B. L., and Holben, B. N. (1997), Sunphotometric measurements of atmospheric water vapor column abundance in the 940-nm band. *J. Geophys. Res.* 102:4343–4352.
- Hansen, J. E., and Lacis, A. A. (1990), Sun and dust versus greenhouse gases: an assessment of their relative roles in global climate change. *Nature* 346:713–719.
- Harrison, L., Michalsky, J., and Berndt, J. (1994), Automatic multifilter rotating shadow-band radiometer: an instrument for optical depth and radiation measurements. *Appl. Opt.* 33:5118–5125.
- Holben, B. N., Kalb, V., Kaufman, Y. J., Tanré, D., and Vermote, E. (1992), Aerosol retrieval over land from AVHRR data—application for atmospheric correction. *IEEE Trans. Geosci. Remote Sens.* 30:212–222.
- Holben, B. N., Setzer, A., Eck, T. F., Pereira, A., and Slutsker, I. (1996), Effect of dry-season biomass burning on Amazon basin aerosol concentrations and optical properties, 1992–1994. *J. Geophys. Res.* 101:19,465–19,481.
- Iqbal, M. (1983), *An Introduction to Solar Radiation*, Academic, San Diego, CA, 390 pp.
- Kasten, F., and Young, A. T. (1989), Revised optical air mass tables an approximation formula. *Appl. Opt.* 28:4735–4738.
- Kaufman, Y. J. (1993), Measurements of the aerosol optical thickness and the path radiance—implications on aerosol remote sensing and atmospheric corrections. *J. Geophys. Res.* 98:2677–2692.
- Kaufman, Y. J., and Tanré, D. (1996), Strategy for direct and indirect methods for correcting the aerosol effect on remote sensing: from AVHRR to EOS-MODIS. *Remote Sens. Environ.* 55:65–79.
- Kaufman, Y. J., Gitelson, A., Karnieli, A., et al. (1994), Size distribution and phase function of aerosol particles retrieved from sky brightness measurements. *J. Geophys. Res.—Atmos.* 99:10341–10356.
- King, M. D., Byrne, D. M., Herman, B. N., and Reagan, J. A. (1978), Aerosol size distributions obtained by inversion of spectral optical depth measurements. *J. Atmos. Sci.* 35: 2153–2167.
- Kneizys, F. X., Shettle, E. P., Abreu, L. W., et al. (1988), Users guide to LOWTRAN 7, AFGL-TR-88-0177, NTIS AD A206773, Air Force Geophysics Laboratory, Hanscom Air Force Base, MA.
- Komhyr, W. D., Grass, R. D., and Leonard, R. K. (1989), Dobson Spectrophotometer 83: a standard for total ozone measurements, 1962–1987. *J. Geophys. Res.* 94:9847–9861.
- London, J., Bojkov, R. D., Oltmans, S., and Kelley, J. I. (1976), *Atlas of the Global Distribution of Total Ozone July 1957–June 1967*, NCAR Technical Note 133+STR, National Center for Atmospheric Research, Boulder, CO, 276 pp.
- Michalsky, J. J. (1988), The astronomical almanac's algorithm for approximate solar position (1950–2050). *Solar Energy* 40:227–235.
- Morys, M., Mims, F. M., III, and Anderson, S. E. (1998), Design, calibration and performance of MICROTOS II handheld ozonimeter, in preparation.
- Nakajima, T., Tanaka, M., and Yamauchi, T. (1983), Retrieval of the optical properties of aerosols from aureole and extinction data. *Appl. Opt.* 22:2951–2959.
- Nakajima, T., Takamura, T., Yamano, M., et al. (1986), Consistency of aerosol size distributions inferred from measurements of solar radiation and aerosols. *J. Meteorol. Soc. Jpn.* 64:765–776.
- Nakajima, T., Glauco, T., Rao, R., Boi, P., Kaufman, Y., and Holben, B. (1996), Use of sky brightness measurements from ground for remote sensing of particulate polydispersions. *Appl. Opt.* 35:2672–2686.
- NOAA/NESDIS (1990), *User Interface Manual Version 1.1 for the GOES, Data Collection System Automatic Processing System (DAPS)*, prepared by Integral Systems, Inc. for NOAA/NESDIS, Contract No. 50-DDNE-7-00037.
- O'Neill, N. T., and Miller, J. R. (1984), Combined solar aureole

- and solar beam extinction measurements. 1: Calibration considerations. *Appl. Opt.* 23:3691–3696.
- Penndorf, R. (1957), Tables of the refractive index for standard air and the Rayleigh scattering coefficient for the spectral region between 0.2 and 20.0 microns and their application to atmospheric optics. *J. Opt. Soc. Am.* 47:176–182.
- Rao, C. R. N., McClain, E. P., and Stowe, L. L. (1989), Remote-sensing of aerosols over the oceans using AVHRR data theory, practice and applications. *Int. J. Remote Sens.* 10: 743–749.
- Reagan, J. A., Thomason, L. W., Herman, B. M., and Palmer, J. M. (1986), Assessment of atmospheric limitations on the determination of the solar spectral constant from ground-based spectroradiometer measurements. *IEEE Trans. Geosci. Remote Sens.* GE-24:258–265.
- Reagan, J. A., Thome, K. J., and Herman, B. M. (1992), A simple instrument and technique for measuring columnar water vapor via Near-IR differential solar transmission measurements. *IEEE Trans. Geosci. Remote Sens.* 30:825–831.
- Russel, P. B., Livingston, J. M., Dutton, E. G., et al. (1993), Pinatubo and pre-pinatubo optical depth spectra: Mauna Loa measurements, comparisons, inferred particle size distributions, radiative effects and relationships to lidar data. *J. Geophys. Res.* 98:22,969–22,985.
- Schmid, B., Matzler, C., Heimo, A., and Kampfer, N. (1997), Retrieval of optical depth and particle size distribution of tropospheric and stratospheric aerosols by means of sun photometry. *IEEE Trans. Geosci. Remote Sens.* 15:172–182.
- Shaw, G. E. (1976), Error analysis of multiwavelength sun photometry. *Pageoph.* 114:1–14.
- Shaw, G. E. (1983), Sun photometry. *Bull. Am. Meteorol. Soc.* 64:4–11.
- Shiobara, M., Hayasaka, T., Nakajima, T., and Manaka, M. (1991), Aerosol monitoring using a scanning spectral radiometer in Sendai, Japan. *J. Meteorol. Soc. Jpn.* 60:57–70.
- Smirnov, A., et al. (1998), Cloud screening and quality control algorithms for the AERONET data base, in preparation.
- Tanré, D., Deuaux, C., Herman, M., and Santer, R. (1988), Radiative properties of desert aerosols by optical ground-based measurements at solar wavelengths. *J. Geophys. Res.* 93: 14,223–14,231.
- Twitty, J. T. (1975), The inversion of aureole measurements to derive aerosol size distributions. *J. Atmos. Sci.* 32:584–591.
- Vermote, E. F., Tanré, D., Deuze J. L., Herman, M., and Morcrette, J. J. (1997), Second simulation of the satellite signal in the solar spectrum, 6S: an overview. *IEEE Trans. Geosci. Remote Sens.* 35:675–686.
- Vigroux, E. (1953), Contribution à l'étude expérimentale de l'absorption de l'oxone. *Ann. Phys.* 8:709.
- Volz, F. E. (1959), Photometer mit Selen-photoelement zur spektralen Messung der Sonnenstrahlung und zur Bestimmung der Wellenlangenabhängigkeit der Dunsttrübung. *Arch. Meteorol. Geophys. Bioklim.* B10:100–131.
- Walker, J. H., Cromer, C. L., and McLean, J. T. (1991), Calibration of passive remote observing optical and microwave instrumentation. In *Proc. SPIE—The International Soc. of Optical Engineering*, 3–5 April, Orlando, FL, Vol. 1493, pp. 224–230.
- Young, A. T. (1980), Revised depolarization corrections for atmospheric extinction. *Appl. Opt.* 19:3427–3428.